Electronic Supplementary Information

Transforming Waste Newspapers into Nitrogen-doped Conducting Interlayers of Advanced Li-S batteries

Chi-Hao Chang, Sheng-Heng Chung and Arumugam Manthiram*

Materials Science and Engineering Program & Texas Materials Institute
The University of Texas at Austin, Austin, TX 78712, USA

Fabrication of nitrogen-doped conducting (NC) interlayers

The NC interlayer was fabricated through a sustainable route. The waste newspapers (The Daily Texan) which are free for all people were cut into small area and immersed into the saturated urea solution for 24 hr. The urea-treated newspapers were directly carbonized at 950 ^{o}C for 3 hr under an inert environment. The resulting NC interlayers were cut into the same size as the sulfur cathode with an area of 1.13 cm^{-2}. The weight of the NC interlayer was less than 2 mg cm^{-2}.

Pure Sulfur cathodes

The pure sulfur cathodes adopted in the advanced Li-S cells directly use commercial sulfur powders as the active material, which avoids the use of complicated nanosynthesis route and corresponding limited sulfur content in the

*Corresponding author. Tel: +1-512-471-1791; fax: +1-512-471-7681.
E-mail address: manth@austin.utexas.edu (A. Manthiram)

preparation of S/C composite cathode. The active-material slurry contained 75 wt.% sulfur (S, Fisher Scientific; purity = 99.5%), 15 wt.% Super P (TIMCAL), and 10 wt.% polyvinylidene fluoride (PVdF, Kureha). The mixture was continuously stirring for 2 days to form a viscous active-material slurry. The obtained active-material slurry was homogeneously tape-casted onto an aluminum (Al) current collector and dried for 24 h at 50 °C. The prepared pure sulfur cathode had a sulfur content of 75 wt.% and sulfur loading of 3.0 mg cm^{-2}. To attain a fair comparison on electrochemical characteristics, the pure sulfur cathodes used in the conventional Li-S cells had the sulfur content of 50 wt.% with sulfur loading of 3 mg cm^{-2}. Specifically, the pure sulfur cathode for conventional cells contained 50 wt.% S, 40 wt.% Super P, and 10 wt.% PVdF.

Cell assembly

The sulfur cathode was dried in an oven at 50 ^{o}C before cell assembly. The electrolyte used in both the advanced Li-S cell and the conventional Li-S cell contained 1.85 M lithium trifluoromethanesulfonate salt ($LiCF_3SO_3$, Acros Organics) and 0.1 M lithium nitrate ($LiNO_3$, Acros Organics) additive in a 1, 2-Dimethoxyethane (DME; Acros Organics)/1, 3-Dioxolane (DOL; Acros Organics) (volume ratio = 1:1). The advanced Li-S cells (CR2032-type coin cells) were

assembled in the order of the sulfur cathode (75 wt.% S), the polymeric separator (Celgard), the NC interlayer, and the Li anode. The sulfur content in the whole cathode including the weight of NC interlayer was 50 wt.%. Therefore, the conventional Li-S cells were assembled with the sulfur cathode (50 wt.% S), the polymeric separator, and the Li anode. The amount of electrolyte in both advanced cells and conventional cells was kept in the same (50 μL).

Characterizations

The microstructure of the prepared the NC interlayers and the morphological changes of the NC interlayers before and after cycling were examined with a field emission scanning electron microscope (FE-SEM) (Quanta 650 SEM, FEI). The energy dispersive spectrometer (EDS) was used for collecting elemental signals and mapping results. The cycled conventional and advanced Li-S cells were dissembled inside an argon-filled glove box to retrieve the cycled NC interlayers and the cycled Li anode. The retrieved cycled samples were cleaned with the DME/DOL co-solvent. The SEM samples were stored in argon-filled sealed vessels before SEM inspection. The porosity analysis was carried out by measuring the nitrogen adsorption and desorption behaviors with an automated gas sorption apparatus (AutoSorb iQ2, Quantachrome Instruments) at -196 °C. The specific surface area was calculated by

the 7-point Brunner-Emmett-Teller (BET) method. The pore-size distributions (PSD) were analyzed by integrating three different PSD models, including (i) the Horvath-Kawazoe (HK) micropore model, (ii) the density functional theory (DFT) micro-to-meso-PSD model, and (iii) the broad Barrett-Joyner-Halenda (BJH) PSD method. The microporosity analysis was calculated by the t-plot method under activated carbon modal and supported by the Dubinin-Radushkevich (DR) equations. Fourier transformed infrared (FT-IR) spectra were recorded on a FT-IR spectrometer (Nicolet iS5, Thermo Fisher Scientific Inc.). All samples were scanned in a wavenumber range of 500 to 4000 cm^{-1}. The spectra of the mixtures were recorded in 16 scans.

Electrochemical examination

The assembled Li-S cells were rested for a half hour before conducting the electrochemical measurements. The cyclic voltammetry (CV) test was carried out with a universal potentiostat (VoltaLab PGZ 402, Radiometer Analytical) between 1.8 and 2.8 V at a scan rate of 0.1 mV s^{-1}. Discharge/charge profiles and cycling stability were recorded with a battery test station (Arbin). All discharge capacities were calculated based on the mass and the theoretical capacity of sulfur in the entire cathode.

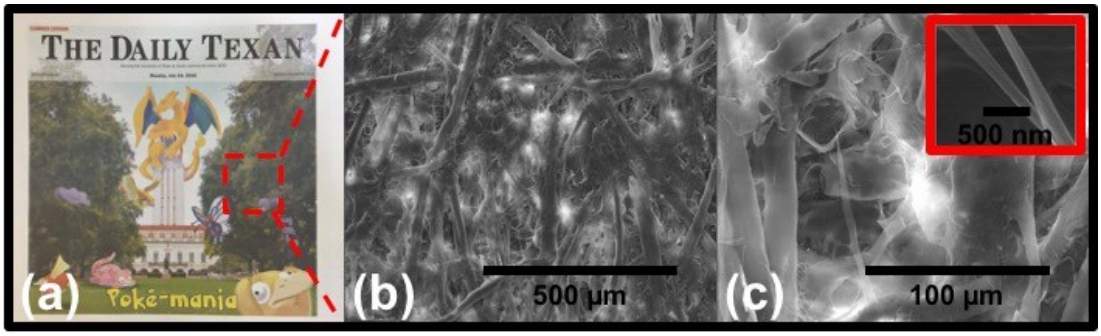

Fig. S1 (a) the photo of waste The Daily Texan. (b and c) SEM images of The Daily Texan.

Fig. S1 shows the photo and microstructure of waste newspapers. The porous architecture constructed by the unique intertwined fibrous structure.

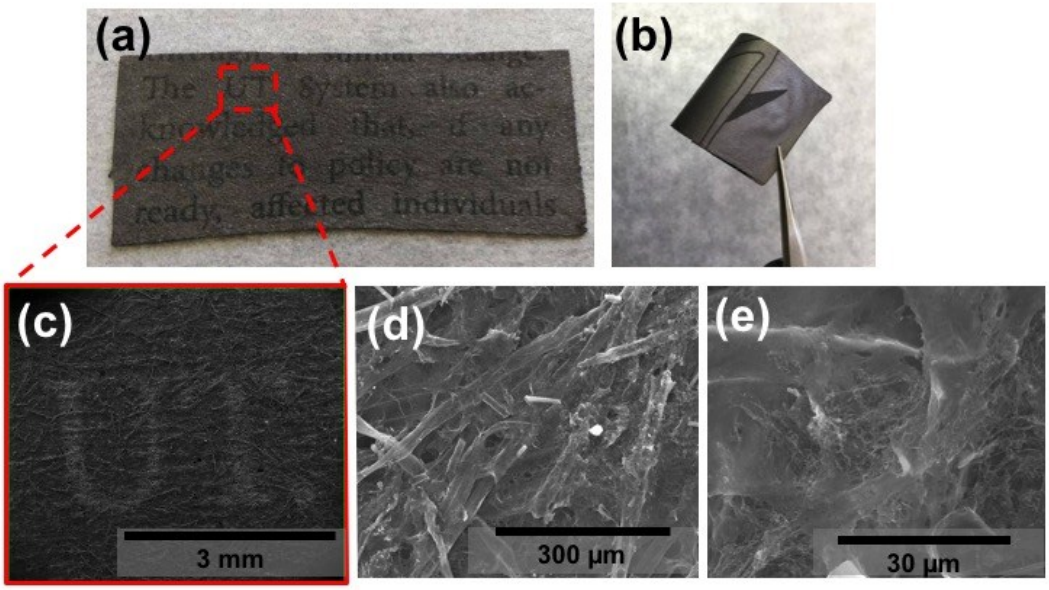

Fig. S2 (a and b) Photographs of NC interlayers. (c – e) SEM images of NC interlayers.

The same interconnected fibrous structure shown in Fig. S1 is maintained after the carbonization process, as shown in Fig. S2. Even the tiny worlds ("UT") in the newspaper are still clearly observed through naked eyes and SEM images. The NC

interlayers also possess good mechanical properties (Fig. S2b) which can cushion the stress originated large morphologic changes of cathode during cycling.[S1]

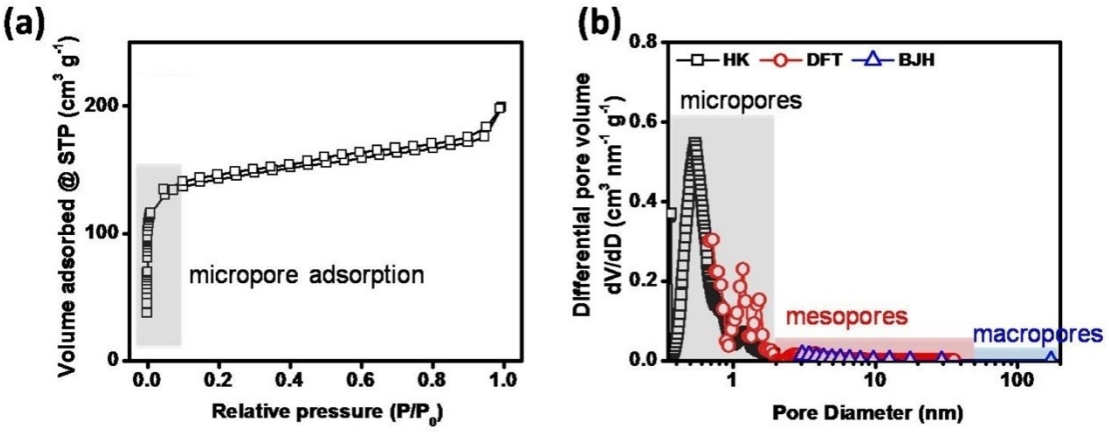

Fig. S3 (a) Nitrogen adsorption-desorption isotherms and (b) pore-size distributions with HK, DFT, and BJH models.

Fig. S3 indicates that the NC interlayer intrinsically possesses abundant micropores. The high microporosity results in the high values of micropore volume and micropore area of, respectively, 0.19 cm^3 g^{-1} and 327 m^2 g^{-1}. This indicates that the micropores contribute almost 80% of the surface area. The high accessible reaction area brought by these micropores improves the polysulfide-trapping capability and the electrochemical-reaction accessibility of the NC interlayer.

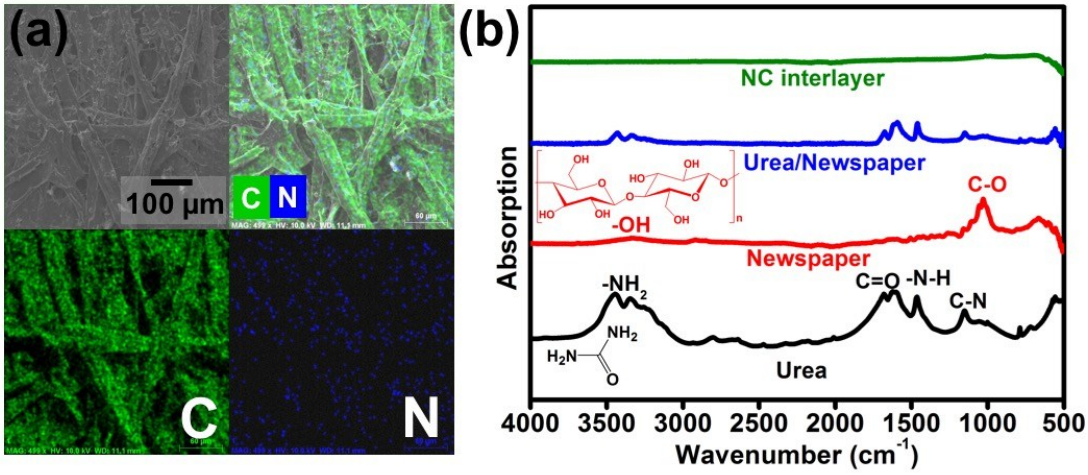

Fig. S4 (a) SEM image and elemental mapping results (carbon: green dots; nitrogen: blue dots) of NC interlayers. (b) FTIR spectra.

Fig. S4a reveals that the nitrogen element originated from urea is successfully doped into the carbon matrix of the NC interlayers.[S2] The FTIR spectra (Fig. S4b) display obvious peaks at 3448 and 3441 cm^{-1} (N-H stretching vibrations), 1689 cm^{-1} (C=O stretching vibration), 1611 cm^{-1} (N-H deformation (bending) vibration), and 1461 and 1146 cm^{-1} (C-N stretching (asymmetric/symmetric) vibrations). These FTIR peaks demonstrate the existence of urea molecules located at the surface of waste newspapers.[S3] A peak at around 1030 cm^{-1} is assigned to C-O bond stretching in the cellulose fibers.[S4] The absence of characteristic peaks in the NC interlayer implies the success in doping nitrogen into carbon matrix of the NC interlayer.

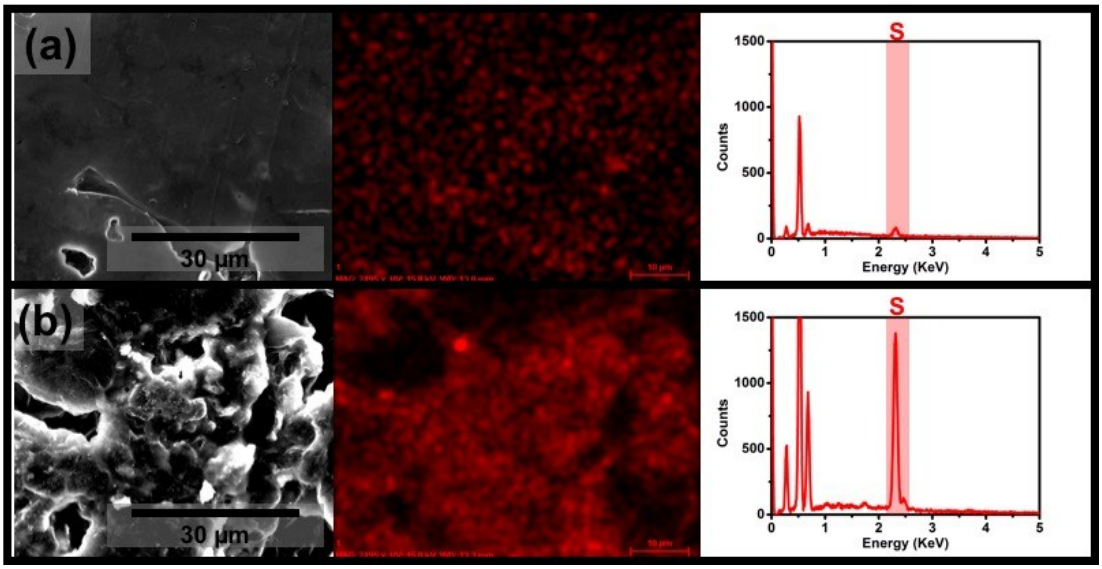

Fig. S5 SEM images of the cycled Li anodes in (a) conventional Li-S cells and (b) advanced Li-S cells.

Fig. S5 shows a huge difference between the cycled Li anodes retrieved from the conventional Li-S battery and the advanced Li-S battery. After cycling, the Li anode in the conventional Li-S cells exhibits strong sulfur signals and thick inactive sulfur-species layer on the surface (Fig. S5a). The formation of these inactive aggregates results from the undesirable reactions between the migrating polysulfides and the Li anode. The cycled anode in the advanced cells, however, remains intact without obvious inactive precipitates on the surface (Fig. S5b). Moreover, the weak sulfur signals on the surface of the cycled Li anode indicates a reduced migration of polysulfides. The results reconfirm that the NC interlayers effectively localize the migrating polysulfides within the cathode region.[S5]

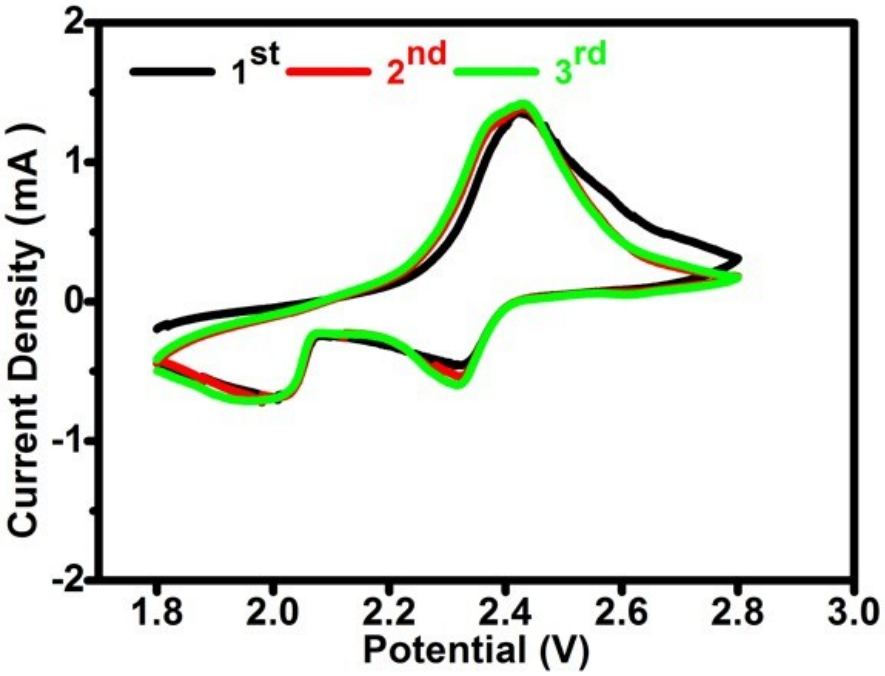

Fig. S6 Cyclic voltammogram of advanced Li-S cells at a scan rate of 0.1 mV s^{-1}.

The redox reactions of the advanced Li-S cells were investigated by the CV test (Fig. S5). Apparently, the insertion of the NC interlayer does not alter the typical redox reactions in the Li-S system. Additionally, the overlapping CV curves also demonstrate that placing the NC interlayer between the sulfur cathode and the porous separator can effective improve the electrochemical performance of the Li-S battery.[S6] This improvement results from the synergistic polysulfide-suppression behaviors of the NC interlayer.

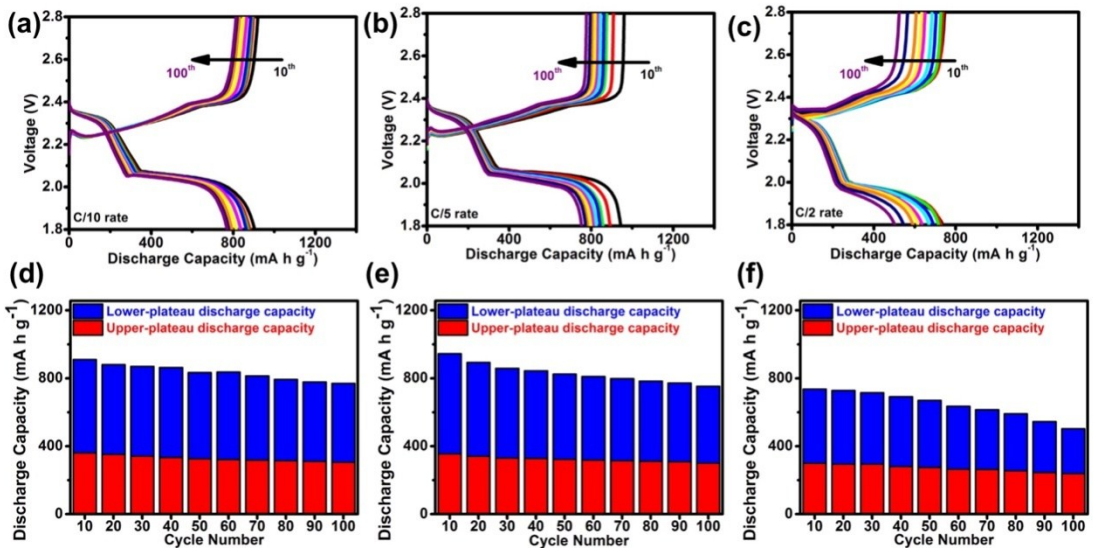

Fig. S7 Discharge/charge curves and reversible Q_H/Q_L of the Li-S cells employing the NC interlayers at (a and d) C/10, (b and e) C/5, and (c and f) C/2 cycling rates.

The voltage profiles of the advanced Li-S cells at various cycling rates are shown in Fig. S6a – c. The curves illustrate that the advanced Li-S cells exhibit typical two-step redox reactions involving the first-stage redox reactions between sulfur and polysulfides and the second-stage redox reactions between polysulfides and sulfides.[S7] The overlapping curves at different rates show that the advanced cells exhibit good rate performance. The Q_H and Q_L values are good indicators of, respectively, polysulfide retention and redox accessibility.[S8] The constant Q_H values (red charts) indicate excellent polysulfide-retention capability of the NC interlayers (Fig. S6d – f). The stable Q_L values (blue charts), on the other hand, imply the excellent redox capability.

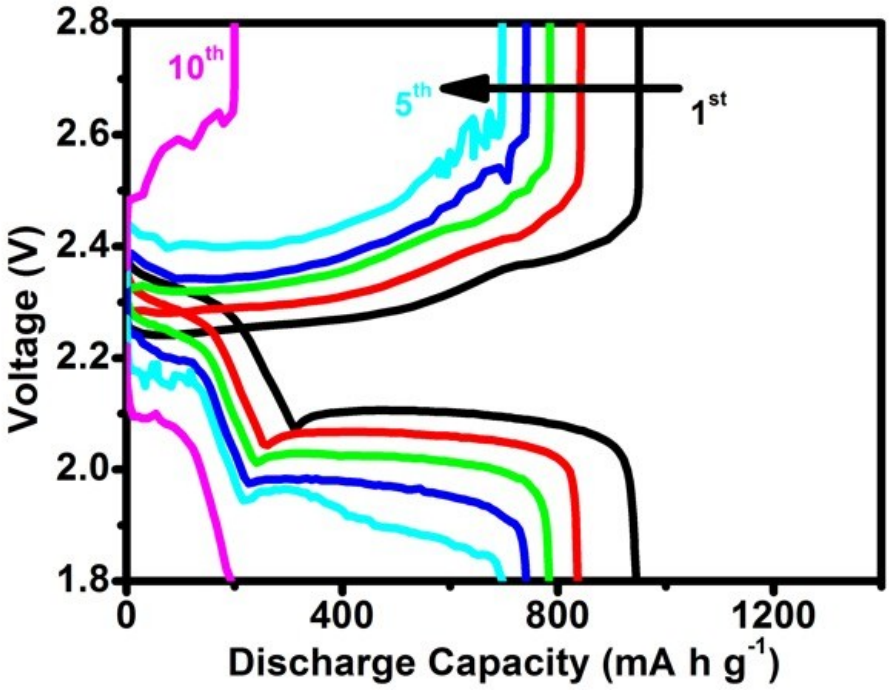

Fig. S8 Discharge/charge curves of the conventional cell at C/10 cycling rate.

In the conventional cell configuration, it is clear that the upper plateaus that indicate the polysulfide formation and migration shrink dramatically in the initial ten cycles (Fig. S7). The severe polysulfide migration leads to the typical fast capacity fade.

Table S1 Comparison of the synthesized interlayers and the interlayers derived from wastes.

Materials	Sulfur loading (mg cm^{-2})	Mass of interlayer (mg cm^{-2})	Initial capacity (mA h g^{-1})	Reversible capacity (mA h g^{-1})	Capacity retention (%)	Reference
TiO_2/Graphene	1.2	0.15	835	685[a]	82	S9
Reduced graphene oxide	3	3	1139	749[b]	66	S10
Mesoporous Carbon	1.7	0.9	1364	1104[c]	81	S11
Polypyrrole nanotube	2.5 – 3	1	1102	712[a]	65	S12
Carbonized Eggshell	3.2	-	1327	1000[b]	75	S13
Carbonized Kimwipes	1.1	1.4	1192	847[c]	71	S14
NC interlayers	3	2	990	753[b]	76	This work

[a] 300 cycles

[b] 100 cycles

[c] 200 cycles

References

S1 A. Manthiram, Y. Fu, S.-H. Chung, C. Zu and Y.-S. Su, *Chem. Rev.*, 2014, **114**, 11751–11787.

S2 T.-N. Ye, W.-J. Feng, B. Zhang, M. Xu, L.-B. Lv, J. Su, X. Wei, K.-X. Wang, X.-H. Li and J.-S. Chen, *J. Mater. Chem. A*, 2015, **3**, 13926–13932.

S3 Z. Piasek and T. Urbanski, *B Pol Acad Sci-Tech X*, 1962, 113–120.

S4 C. Wang, Y. Li, X. He, Y. Ding, Q. Peng, W. Zhao, E. Shi, S. Wu and A. Cao, *Nanoscale*, 2015, **7**, 7550–7558.

S5 C.-H. Chang, S.-H. Chung and A. Manthiram, *Small*, 2016, **12**, 174–179.

S6 M. K. Rybarczyk, H.-J. Peng, C. Tang, M. Lieder, Q. Zhang and M.-M. Titirici, *Green Chem.*, 2016, **18**, 5169-5179.

S7 C. Barchasz, F. Molton, C. Duboc, J.-C. Leprêtre, S. Patoux and F. Alloin, *Anal. Chem.*, 2012, **84**, 3973–3980.

S8 X. Yang, N. Yan, W. Zhou, H. Zhang, X. Li and H. Zhang, *J. Mater. Chem. A*, 2015, **3**, 15314–15323.

S9 Xiao, Z. Yang, L. Wanag, H. Nie, M. ’e Zhong, Q. Lai, X. Xu, L. Zhang and S. Huang, *Adv. Mater.*, 2015, **27**, 2891–2898.

S10 X. Wang, Z. Wang and L. Chen, *J. Power Sources*, 2013, **242**, 65–69.

S11 J. Balach, T. Jaumann, M. Klose, S. Oswald, J. Eckert and L. Giebeler, *J. Phys. Chem. C*, 2015, **119**, 4580–4587.

S12 G. Ma, Z. Wen, Q. Wang, C. Shen, P. Peng, J. Jin and X. Wu, *J. Power Sources*, 2015, **273**, 511–516.

S13 S.-H. Chung and A. Manthiram, *Adv. Mater.*, 2014, **26**, 1360–1365.

S14 S.-H. Chung and A. Manthiram, *Chem. Commun.*, 2014, **50**, 4184–4187.